ACS OMEGA

Open Access



http://pubs.acs.org/journal/acsodf

Article

# Analysis and Application of Poly(vinyl alcohol) (PVA) and Polyacrylonitrile (PAN) Nanofiber Membrane-Based Triboelectric Nanogenerators

Subalakshmi Pragalathan and Velmurugan Venugopal*

Cite This: *ACS Omega* 2024, 9, 37802−37813

Read Online

ACCESS | Metrics & More | Article Recommendations

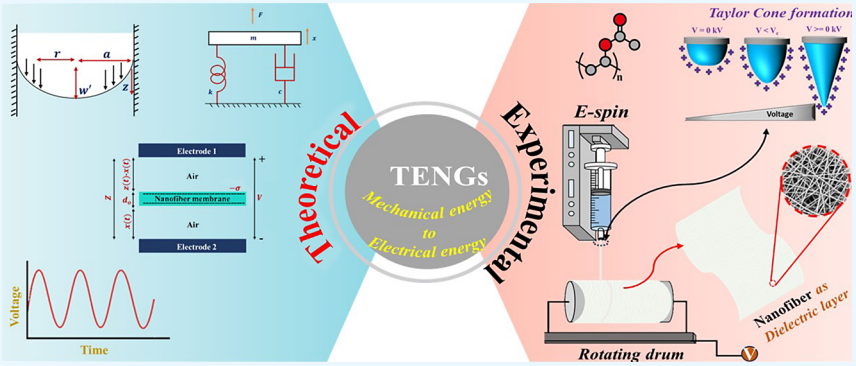


**ABSTRACT:** The triboelectric property of materials is used to harvest energy from intentional or nonintentional sources of vibration. Contact mode freestanding dielectric based nanogenerators (CFTENGs) have many advantages when compared with other modes of triboelectric nanogenerators. The property of dielectric materials plays an important role in the energy harvesting process. In this work, we aim to fabricate nanofiber membranes of poly(vinyl alcohol) (PVA) and polyacrylonitrile (PAN) and study their properties for CFTENGs. The morphology and porosity of both membranes were tested experimentally. The mechanical property is modeled with a representative volume element (RVE) technique to understand its deflection behavior. In addition, an electromechanical model is developed to predict and analyze the behavior of those membranes in the energy conversion process. Our research reveals that the PAN dielectric layer achieves a maximum open circuit voltage of 192 kV compared to the PVA dielectric layer (2.2 kV) in the CFTENG system. In comparison, the dielectric layer of the PAN nanofiber membrane reflects its flexibility to generate electrical energy in a CFTENG with the effect of contact electrification and electrostatic induction under various sources of unused energies for a wide range of applications. Moreover, the same methodology is applied to various sources of vibration, and their performance is reported. With an appropriate power management circuit, we can design a PAN membrane-based TENG for various applications.

## 1. INTRODUCTION

The widespread use of electronic gadgets makes sense in the development of sustainable power sources. Macro and microelectronic devices are powered using chemical batteries that are hazardous to the environment and have a limited lifetime.[1,2] In this context, converting unused energy into electrical energy is an important topic for scientists.[3−7] A nanogenerator based on the triboelectric effect of contact electrification and electrostatic induction from mechanical energy to generate electric energy was reported in 2012.[8] Triboelectric nanogenerators (TENGs) have broad prospects such as high output energy, high charging and discharging rates, low maintenance, high scalability, simple structures, free of pollution, and cost-effective technology.[9−12] TENGs were investigated universally with diverse energy sources, materials, and operation modes due to their low weight and easy fabrication to implement into various applications.[13,14] The power supplied from TENGs was demonstrated as a sustainable power source for portable electronic devices, batteries of mobile phones, and other low power systems.[15−17] In common, TENGs contain an electrode attached with a dielectric layer and have limitations in their applications. In a freestanding triboelectric nanogenerator (FTENG), contact

**Received:** April 19, 2024
**Revised:** July 9, 2024
**Accepted:** July 17, 2024
**Published:** August 27, 2024

separation of electrodes with a stacked structure of a dielectric layer will restrict the electric field within stationary electrodes which can be represented as a contact mode freestanding triboelectric layer-based TENG (CFTENG).[18] The CFTENG mode has been widely ulitized in wind energy harvesting and self-powering electronics due to its advantages of easy fabrication, low cost, sustainability, and single triboelectric layers without attached electrodes compared to other modes like contact mode and sliding mode TENGs.[18−20] To design a TENG for a particular application, the theoretical work is considered as a basic requirement to analyze its electrical output performance. Moreover, it is necessary to understand the mechanical properties of the dielectric layer for TENG-related applications.

The most preferred TENG materials are polyimide (PI), polytetrafluoroethylene (PTFE), polypropylene (PP), polydimethylsiloxane (PDMS), polyvinylidene fluoride (PVDF), polyvinyl chloride (PVC), polyacrylonitrile (PAN), cellulose, polyurethane (PU), and poly(vinyl alcohol) (PVA). These polymeric materials were structured differently such as nanofibers, thin films, and aerogels to analyze the performance of TENGs.[21] The performance of the TENGs depends on the surface characteristics of the triboelectric layer. The surfaces with structures like pyramids, sheets, wires, pores, and nanowires exhibit better performance than unpatterned surfaces.[22] The interfacial micro and nanostructure deformation of triboelectric layers has an impact on the force and voltage relationship in TENGs.[23,24] Several research studies are ongoing on using nanostructured triboelectric layers for a wide range of self-powering systems.

Nanofiber structures were developed for numerous applications including energy harvesting technologies owing to its parallel advantages such as high surface volume ratio, lightweight, flexible, and porous structure.[25,26] Nanofiber structured materials can be fabricated using the electrospinning technique due to their ease of fabrication.[27] Typically, nanofiber membranes have the strong potential of providing stable and repeated signals with consistent time intervals.[28] Among polymer materials in triboelectric series, PVA and PAN polymers were chosen based on their functional groups. Poly(vinyl alcohol) (PVA) and polyacrylonitrile (PAN) polymers have the attractive polar groups namely a hydroxyl group (−OH) and a nitrile group (−CN) respectively.[29] The PVA and PAN-based nanofiber membranes were widely utilized in filtration, wound dressing, photocatalytic degradation, and tissue engineering applications due to their excellent characteristics.[30−34]

Moreover, electrospun PVA and PAN-based nanofiber membranes were investigated as a friction layer in various kinds of TENG applications due to their flexibility, ultrathin nature, and stretchability.[35−38] Nanofiber-based TENGs have been developing to generate electricity with a wide range of deformations such as twisting, knee bending, holding, deflection by breathing, and friction by human motions (running, walking, and jumping).[39−41] Therefore, along with the material selection, material structure and the mechanical properties of materials will play an important role in achieving the stable electrical output response of TENGs under external forces. In our proposed CFTENG mode, the dielectric layer will deflect back and forth to make contact and separate with top and bottom electrodes under external forces and will generate power. This kind of mode has been emerging in wind energy harvesting; authors generate the output voltage based on fluttering of dielectric films to make contact and separate with top and bottom electrodes under different ranges of wind flow as external mechanical forces with various kinds of structural designs.[42]

As a consequence, there is a need to investigate and understand the mechanical properties of the membrane as a dielectric layer prior to practical applications in the CFTENG mode. The mechanistic studies of thin nanofibers using instrumentation have limitations due to the fine nature of the nanofibers, which can easily be damaged during testing and it may be expensive sometimes and complex.[43] The numerical analysis is preferred to predict the results accurately and can be implemented in future applications. The mechanical behavior of membranes may vary based on the orientation of internal fibers, diameter of single fibers, and porosity of membranes. The mechanical properties of nonwoven-structured nanofiber membranes can be evaluated with the structural geometry parameter of membrane using the representative volume element (RVE) technique among other models due to the complicated structure of nanofibers. This technique is to study the mechanical behavior of intricate structures of fibers in the membranes on a micro scale to obtain macro scale resultants under uniaxial forces.[44−46] In addition, the dynamic behavior of the membranes was simulated and analyzed by integrating the electromechanical model of single degree of freedom (SDOF) with TENGs under a standard step load. This simulation facilitates an understanding of the connection between the movement of a dielectric layer and electrical efficiency under a frequency response and the damping effect of triboelectric layers. The authors examined the dynamic movement of triboelectric layers under vibration of the TENG system to understand the electrical efficiency by coupling the electromechanical model with the system.[47,48]

In this work, the objective is to analyze the deflection behavior and electrical performance of electrospun nanofiber membranes to utilize as a dielectric layer in the CFTENG mode for a stable mechanical to electrical energy conversion process. Experimentally, we spun the pristine polymer materials such as PVA and PAN as nanofiber membranes from the electrospinning unit and studied their morphology, fiber orientations, and porous nature. Theoretically, the first part of the analytical work has detailed information on the mechanical behavior such as uniform bending under a uniaxial force and the damping effect of membrane under vibration from force using simple, and existing strategies of RVE methodology and electromechanical coupling model for the CFTENG mode, respectively. The second part involves analyzing the electrical characterization of nanofiber membranes using a fundamental theoretical concept based on the CFTENG mode. In the future, this simple and flexible CFTENG system has been constructed to elucidate the power generating principle with time dependent and independent characteristics.

## 2. EXPERIMENTAL SECTION

**2.1. Materials.** Poly(vinyl alcohol) (PVA) with molecular weight of 89 000−98 000 g/mol, polyacrylonitrile (PAN) with molecular weight of 150 000 g/mol, and the DMF solvent were purchased from Sigma-Aldrich and used without any modification.

**2.2. Fabrication of the Nanofiber Membrane.** To fabricate the membrane by electrospinning, the corresponding polymeric solution was prepared. For the PVA membrane, 10


https://doi.org/10.1021/acsomega.4c03625
ACS Omega 2024, 9, 37802−37813

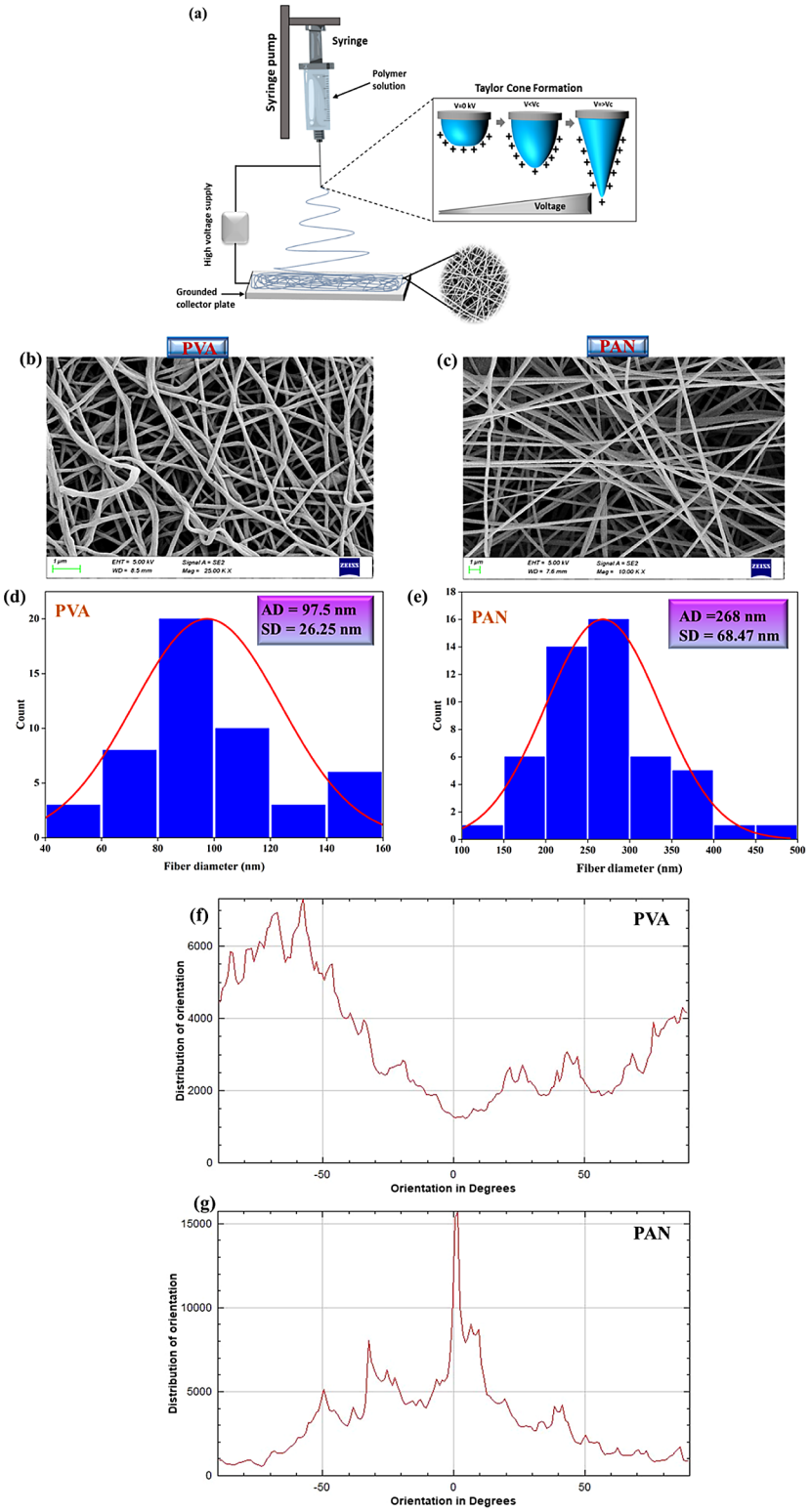


**Figure 1.** (a) Schematic of electrospinning technique. (b,c) SEM images of PVA and PAN nanofiber membranes. (d,e) and (f,g) Their corresponding fiber diameter distribution (AD - average diameter of fiber; SD - standard deviation of fiber diameter) and fiber orientation distribution.

wt % PVA powder was dissolved in hot water by maintaining at 70 °C overnight to prepare the solution. For the PAN membrane, 6 wt % PAN powder was dissolved in DMF as the solvent at room temperature overnight to prepare the homogeneous solution.

As shown in Figure 1a. the solution of PVA and PAN is loaded using a flow pump controller. Here, with a voltage of 22 kV, both PVA and PAN nanofiber membranes were fabricated on the drum collector with a distance of collector-to-needle tip of 12 cm and a solution flow rate of 0.5 mL/h at room temperature in an electrospinning instrument. The nanofibers



https://doi.org/10.1021/acsomega.4c03625
ACS Omega 2024, 9, 37802−37813

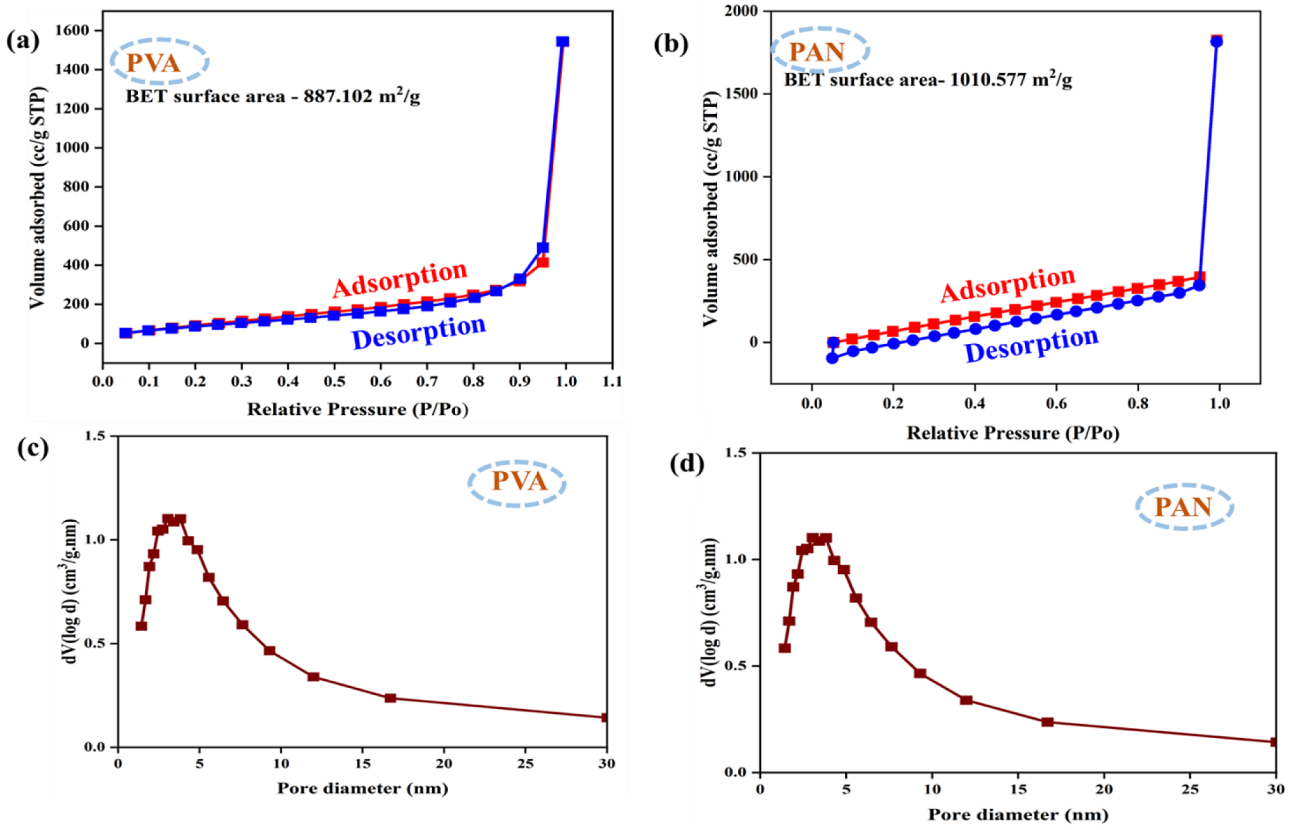


**Figure 2.** (a,b) Nitrogen adsorption−desorption isotherm profiles of PVA and PAN membranes. (c,d) Pore size distribution curve of PVA and PAN.

were spun on aluminum (Al) foil, which is wrapped on a collector. The inset image of Figure 1a represents the spun nanofiber membrane.

**2.3. Morphological Studies.** SEM analysis was performed to analyze the morphology, fiber diameter, and fiber orientation distribution (FOD) of the membrane. Figure 1 presents the analysis of membrane morphology, fiber diameter, and fiber orientation by showing the SEM images of membranes. The PVA and PAN fibers were aligned randomly without any defects such as beads and strings, which can be confirmed from Figure 1b,c. The fibers without beads have a high tensile strength due to their higher cohesion points. The average diameter (AD) of fiber was measured to be 97.5 and 268 nm for PVA and PAN nanofiber membranes respectively using IMAGE J software. The standard deviation (SD) of PVA and PAN are 26.25 and 68.47 nm, respectively. The majority of PVA fibers are in the range of 60−120 nm, and PAN fibers are in the range of 150−350 nm, as shown in Figure 1d,e. The orientation of the fiber was obtained as shown in Figure 1f,g and analyzed using Orientation J to predict its mechanical behavior. It was observed that the maximum count of nanofibers aligned in the same direction (0°) in the PAN membrane compared to the PVA membrane where the nanofibers were oriented randomly (50° and −50°). The formation of aligned nanofibers is due to the variation in the conductivity of the solution.[49] A stable charged jet path is formed if the polymer solution has high conductivity. The PAN solution has higher conductivity (16 500 $\mu$S/cm) than PVA (1275 $\mu$S/cm).[50,51] So, the PAN nanofibers are more aligned.[50,51] The aligned nanofiber membrane has higher mechanical properties than the randomly oriented nanofibers.[52,53] Hence, the PAN membrane has higher mechanical properties in comparison to PVA membrane.

**2.4. BET Specific Surface Area Analysis.** The surface area and pore size distribution of the spun PVA and PAN nanofiber membranes were analyzed using the nitrogen ($N_2$) adsorption and desorption measurements (Brunauer−Emmett−Teller, BET) carried out at 77K temperature.

Figure 2 shows the nitrogen ($N_2$) adsorption and desorption isotherms of PVA and PAN membranes analyzed to determine the specific surface area of BET and pore size membranes. The isotherm profiles (Figure 2a,b) of PVA and PAN resemble the type IV isotherm under IUPAC classification, and its relative pressure hysteresis curve is close to unity, indicating the mesoporous nature of membranes.[54−56] The surface areas of PVA and PAN membranes obtained from the BET test are 887.102 and 1010.577 $m^2/g$, respectively. From the Barret−Joyner−Halenda (BJH) method, the distribution of pore size was measured for fabricated nanofiber membranes. The PVA membrane has the porous ranging between 1.5 and 11 and 16 nm whereas the PAN membrane has pores of 1.4−11 nm, 16, and 29 nm. From the PVA and PAN curves as shown in Figure 2c,d, the ranges of pore size indicated the micropores or mesopores nature. Moreover, the calculated average pore diameter of PVA and PAN membranes further confirms the mesoporous nature of membranes with values of 5.24 and 6.6 nm, respectively. The pore volumes of PVA and PAN membranes are 2.484 and 3.127 cc/g, respectively.

## 3. RESULTS

**3.1. Theoretical Analysis of the Nanofiber Membrane.** The electrical performance of the TENG system is dependent


https://doi.org/10.1021/acsomega.4c03625
ACS Omega 2024, 9, 37802−37813

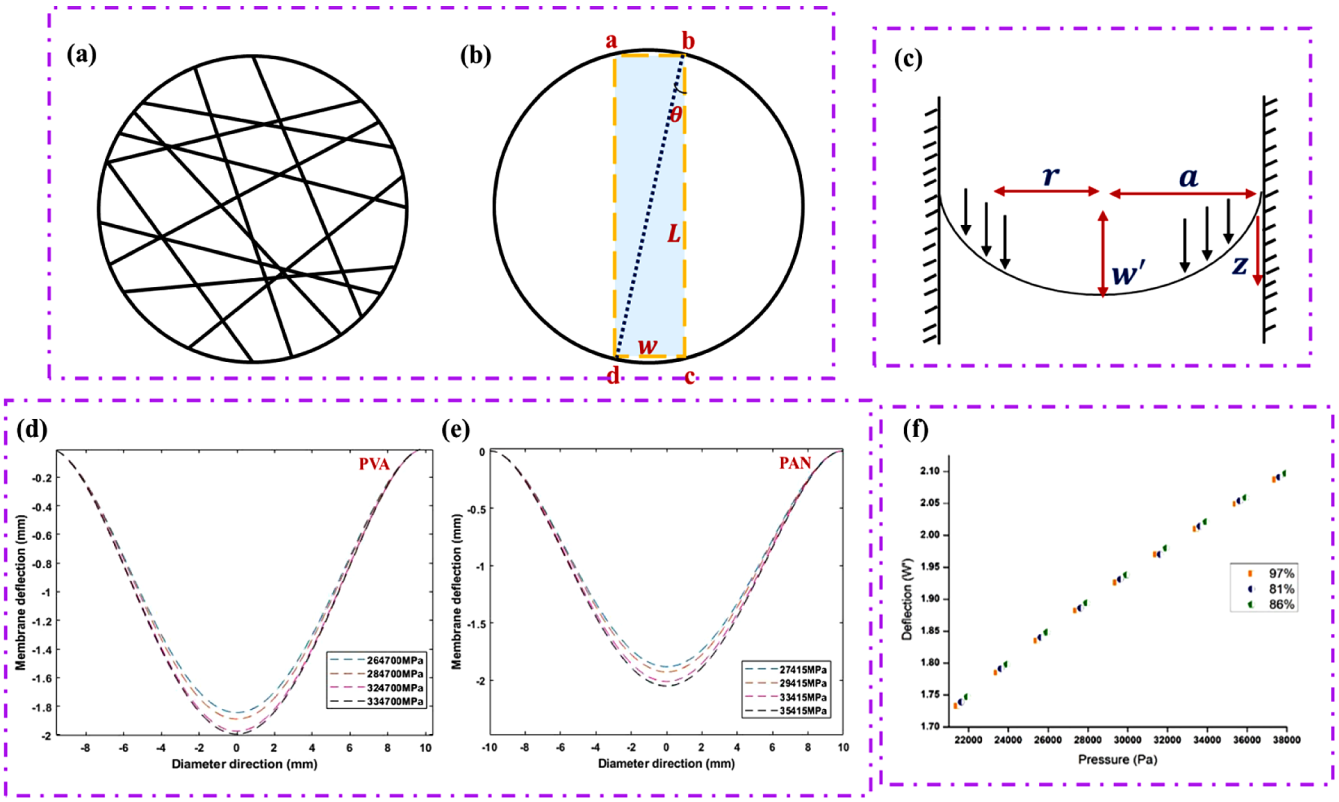


**Figure 3.** (a) RVE diagram of the membrane. (b) Schematic of RVE of nanofiber membrane. (c) Deflection of the circular membrane under a uniform load. (d,e) Deflection profile of PVA and PAN nanofiber membranes under uniform force. (f) Influence of porosity in deflection of the PVA membrane.

on the deflection behavior of the dielectric tribolayer under the external force. It is necessary to understand the mechanical characteristics of the nanofiber membrane.

*3.1.1. Representative Volume Element Method and Deflection Studies of the Nanofiber Membrane.* In this section, the uniform bending of nanofiber membranes under a uniaxial load is analyzed using the representative volume element (RVE) methodology. RVE adopts a process of taking into account a statistically homogeneous representation of a heterogeneous material to analyze the mechanical behavior. In our analysis, the RVE modeling of nanofibers include the factors affecting mechanical behaviors such as porosity, fiber alignment, dimensions of single nanofiber and membrane.[57,58] The analysis is based on assumptions such as the internal structure of the membrane has randomly aligned fibers with the same fiber diameter without any beads, as revealed in Figure 3a. The membrane is circular in shape and is analyzed for the tensile relationship in rectangular RVE cut. The analysis details are discussed below.

The rectangular part of the membrane, which is shown as a colored area in Figure 3b with the parameters such as $L$ as the length and $W$ as the width, forms an RVE unit cell. Those fibers with the ends of overlaying and coinciding in the cross-section of membranes will contribute to resist the given tensile force owing to its insignificant adhesion between the nanofibers. Since there are fibers in a particular portion, the testing outcomes of this tensile test will depend on the fragment of nanofibers that will be the actual area of abcd of the membrane as shown in Figure 3b.[59]

Thus, the fragment of nanofibers can be represented by,

$$\tau(l) = \frac{A_l}{A_\mu} = \frac{L \cdot W}{L^2} = \frac{W}{L} \tag{1}$$

where, $A_l$ is the area of the membrane and $A_\mu$ is the RVE area.

Finding the tensile stress using eq 1 involves membrane thickness ($T$) of RVE, the stress of individual fibers ($\sigma_f$), and porosity ($P$). The stress ($F$) of a tensile membrane including the RVE cut area stretches in a direction and can be obtained using eq 2.

$$F = \frac{\sqrt{2}\,TW(1-P)\sigma_f}{\pi} \int_0^\theta \cos \propto \mathrm{d}\alpha \tag{2}$$

Figure 3c shows that the clamped circular membrane (radius, $a$) has an out of plane behavior ($W'$) under a uniform loading, and expression $z$ represents the out of plane deformation.[60,61]

For finding the deflection ($W'$) of the membrane for an applied force, eqs 1 and 2 can be developed and used.

Since our sample is circular in shape, it results in the deflection of

$$w' = a\sqrt[3]{\frac{1{\cdot}435Pa}{EL}\frac{1-\nu^2}{2.08+4\nu-1{\cdot}2\nu^2}} \cdot \cos\left(\frac{\pi r}{2a}\right) \tag{3}$$

Eq 3 involves the pressure ($P$), young's modulus ($E$), the thickness of membrane ($L$), poisson's ratio ($\nu$), and membrane radius ($a$). The tensile strength of the nanofiber membrane can be analyzed for various porosities, thicknesses, and sizes.

The deflection of the membrane has a contribution of every single nanofiber. The membrane's deflection is found



https://doi.org/10.1021/acsomega.4c03625
ACS Omega 2024, 9, 37802−37813

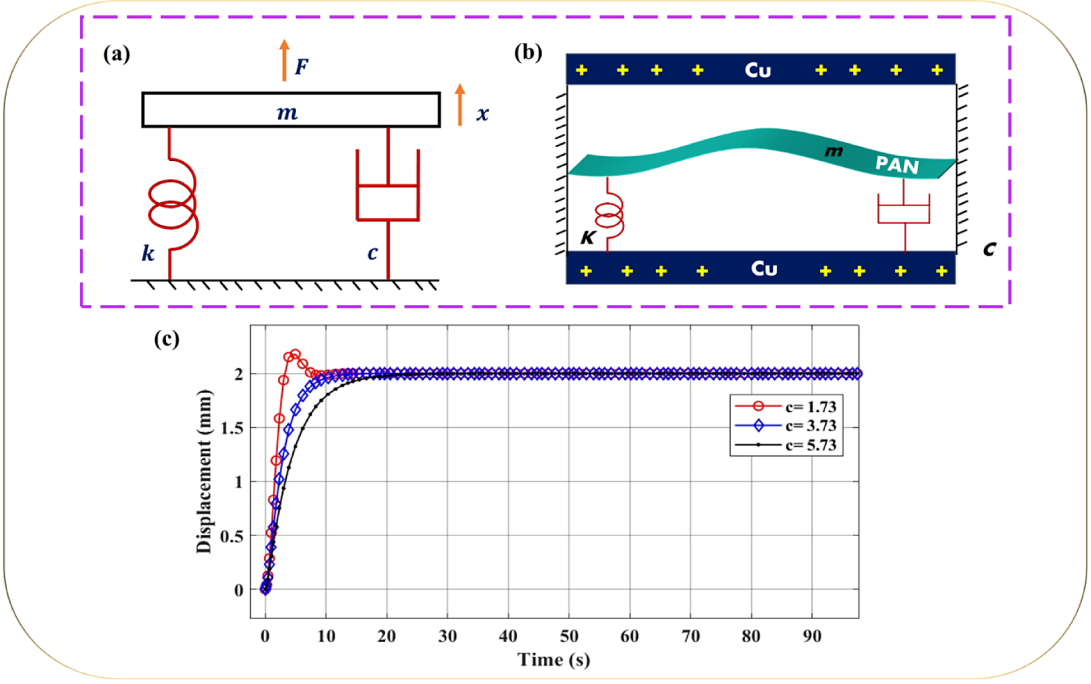


**Figure 4.** (a) Equivalent SDOF model for the CFTENG. (b) Schematic illustration of SDOF model of dielectric CFTENG. (c) Simulated time response of the nanofiber membrane.

maximum at the center for a uniform load as shown in Figure 3c. This profile is based on eq 3 as shown in Figure 3c. Both membranes show uniform bending at the center, and a similar profile is observed. We vary the force acting on it, and the maximum displacement formed is to be 2 mm at a force of 334 700 and 35 415 MPa for PVA and PAN membranes, respectively. According to eq 3, it can be observed that the effect of Young's modulus of the membrane plays an important role in the bending behavior which is represented in Figure 3d,e. Based on eq 2, the deflection is directly proportional to the porosity. So, we anticipated high porosity in both the membranes. The predicted values are shown in Figure 3f. For both PVA and PAN membranes, the deflection decreases with respect to the load. For instance, 86% of the porosity membrane yields a deflection of 2 mm under a pressure of 32 935 Pa.

*3.1.2. Time Response Analysis of the Nanofiber Membrane.* Furthermore, our TENG model is coupled with electromechanical modeling to simulate the dynamic response of the electrospun membrane under a force as represented in eq 4. Here, the system can be modeled by single degree of freedom (SDOF), and there is a strong coupling between the electrode and the dielectric in terms of energy conservation. This model is used to predict the maximum output energy under ideal conditions of a certain TENG.[62,63] The equivalent SDOF model of the CFTENG is represented in Figure 4a.

The SDOF model suitably represents the behavior of the membrane's deflection due to the application of force and it consists of three elements such as mass ($m$) with the support of spring constant ($k$) and damping coefficient ($c$) as shown in Figure 4b.

The governing equation for the system is

$$m\frac{d^2x}{dt^2} + c\frac{dx}{dt} + kx = f \tag{4}$$

$$\frac{md^2x}{dt^2} = f - \frac{cdx}{dt} - kx \tag{5}$$

$$\zeta = \frac{c}{2\sqrt{m}\,k} \tag{6}$$

$\zeta$ is a damping ratio; we tried to investigate the time response of the film for various values of $m$, $k$, and $c$. The classical form of outputs can be grouped under these three categories: (i) undamped, (ii) underdamped, and (iii) overdamped systems based on the damping coefficient ($\zeta$). The relationship can be realized using eq 6 for the nanofiber membrane.

We subject the membrane to a step input and analyze the response. We could pick up three distinct cases, $\zeta > 1$, $\zeta = 1$, $\zeta < 1$ as shown in Figure 4c. By applying the force ($F$) of 2.5 N, the displacement of the membrane has been carried out with constant values for the parameters $m$ as 0.6 g, $k$ as 1.25 N m$^{-1}$, and varying the $c$ as 1.73, 3.73, and 5.73 g/s. The resulting graph indicates an underdamped system that gives a fast response when compared to others. The drawback of the membrane is that it will overshoot and vibrate when it is closer to the electrode. So, it may need time to settle. There could not be a regular electrical output at the time of contact between electrodes.

In other cases, when $\zeta > 1$ is an overdamped system without any oscillation, but it takes time to reach the output; hence, the membrane will move slowly and the derived voltage response also becomes slow. The intermediate is $\zeta = 1$, which is critically damped and this also suffers in poor response time but still it is better than an overdamped system. For a continuous analysis, we repeated the load based on the time response and results as shown in Figure 4c.

*3.1.3. Spring Constant Studies of the Nanofiber Membrane.* The deflection of the nanofiber membrane depends on its flexibility nature, and it was challenging with


https://doi.org/10.1021/acsomega.4c03625
ACS Omega 2024, 9, 37802−37813

its porosity. To predict the flexibility of the membrane, the spring constant study is carried out in this section. The spring constant of the membrane can be studied with dependence on porosity of it as shown in Figure 5. This study helps to

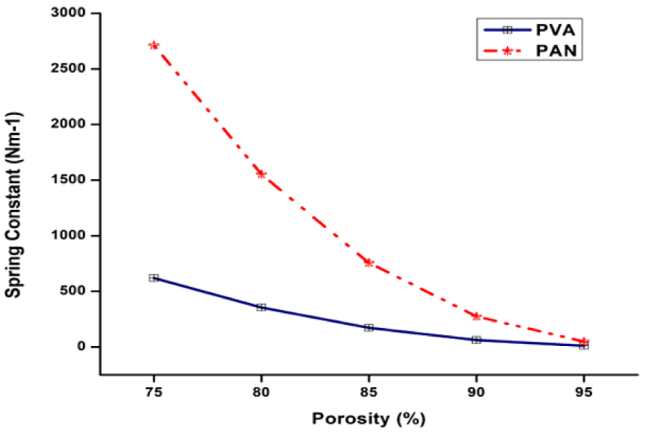


**Figure 5.** Variation of the spring constants of PVA and PAN nanofibers with respect to porosity.

fabricate the appropriate nanofiber membrane, which is attributed to achieve quick and dynamic response of membrane in the TENG system. The spring constant ($K$) of the porous membrane is calculated using eq 7 with varying $P$ based on the value of the spring constant ($K_0$) of the nonporous structure.[64,65]

$$K = K_0{}^{*}(1 - P)^{m} \tag{7}$$

where the spring constant $K_0$ values of nonporous PVA and PAN membranes are 19 821.2 and 86 800 N m$^{-1}$ respectively. $m$ is the power exponent that controls the spring constant rate with the porosity.

The porosity of the membrane has an inverse relationship with the spring constant. Since we have the possibility of variation in the porosity of the membrane, it will affect the spring constant. At the same time, due to changes in porosity, the damping of the membrane will also vary.

**3.2. Analysis of CFTENG Structure.** In this section, the electrical performance of our proposed TENG mode is analyzed. The working mechanism is represented in Figure 6a.

In the contact mode freestanding TENG (CFTENG), the dielectric is sandwiched with suitable spacers between two electrodes. In a normal state, the dielectric layer and two electrodes are at a particular distance and have no charges on their surfaces. After the external force is applied, the membrane surface will deflect slowly against an electrode to make contact between them. An equal magnitude of oppositive charges is created on their surfaces due to the contact electrification effect (Figure 6a.i). When the dielectric layer is partially separated from an electrode, the potential difference will form between them, which makes the charges flow from one electrode to another electrode through the external circuit and generate the current due to the electrostatic induction effect (Figure 6a.ii). When the dielectric layer is completely separated from an electrode, an electrostatic equilibrium can be obtained, and there is no movement of charges through the external circuit (Figure 6a.iii). The dielectric layer and another electrode make contact again, and the charges flow back through the external circuit and generate current (Figure 6a.iv). When the dielectric layer makes contact between the electrodes repeatedly, the charges will move back and forth from one electrode to another electrode through the external circuit and generate an alternative current (AC) signal. The electrical output response of this TENG under a periodic motion is modeled using LTspice.

*3.2.1. V– Q–x Relationship in the TENG.* The membrane and electrodes arranged in the TENG can be modeled with three capacitors in series whose equivalent capacitance is given by the CFTENG. The CFTENG is based on a lumped component representation of a variable capacitor.

Based on the conventional theory of capacitance with $d_0$ is the effective thickness, $S$ is the area, $x(t)$ is the time dependent distance of the dielectric layer, the capacitances ($C_1$, $C_2$, and $C_3$) between the electrodes as the total capacitance ($C_{TENG}$) of CFTENG can be expressed in eq 8.

$$C_{TENG} = \frac{\varepsilon_0 S}{d_0 + x(t)} \tag{8}$$

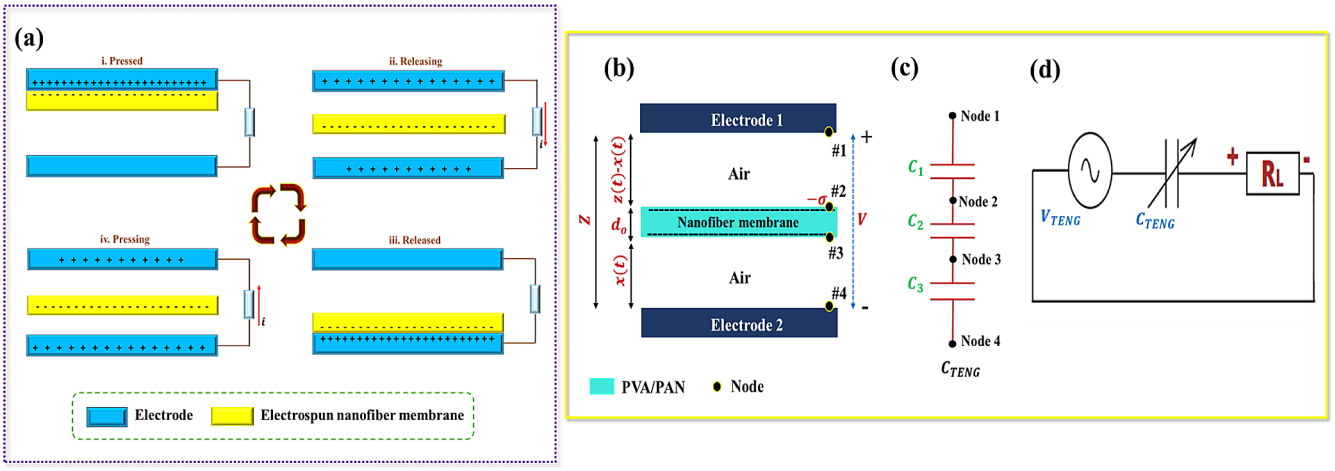


**Figure 6.** (a) Working mechanism of the CFTENG. (b) Typical theoretical model of dielectric layer of CFTENG. (c) Equivalent circuit model of an electrostatic system of dielectric layer of CFTENG. (d) An equivalent circuit of the TENG.



https://doi.org/10.1021/acsomega.4c03625
ACS Omega 2024, 9, 37802−37813

The voltage with charge density $\sigma$ depends on the nanofiber membrane (dielectric) distance $x(t)$ as represented in eq 9, and the equation of open circuit voltage ($V_{oc}$ or $V_{TENG}$) of the CFTENG system is represented in Figure 6b.

$$V_{oc} = \frac{\sigma}{\varepsilon_0} x(t) \tag{9}$$

The output voltage ($V$) of any TENG mode is systematically examined using the below equation which involves the basic $V-Q-x$ relationship.[67]

$$V = -\frac{1}{C_{TENG}} Q + V_{oc}(x) \tag{10}$$

This $V-Q-x$ relationship equation has capacitance ($C$) between the electrodes, transferred charge ($Q$) between electrodes, and open-circuit voltage ($V_{oc}$) of our mode which is a function of separation distance ($x$) between the electrodes.

From eq 10, the equivalent circuit of a TENG is modeled as a series connection of voltage source ($V_{TENG}$) and time varying capacitance ($C_{TENG}$) which is represented based on lumped-component circuit theory as shown in Figure 6d.[66]

*3.2.2. Electrical Output Characteristics of PVA and PAN Nanofiber Membranes.* Based on the mechanical studies and the time response, we selected a critically damped mode of response and applied the same to predict the output of the TENGs.

We applied a periodic input to the whole TENG system and maintained the distance between the electrodes and the dielectric layer. Based on the magnitude and frequency of the periodic input, the output is analyzed. Table 1 lists the parameters used for simulation.

**Table 1. Parameters Used to Simulate CFTENG**

| parameters | PVA dielectric layer | PAN dielectric layer |
|---|---|---|
| dielectric | $\varepsilon_r$ = 1.99, $d$ = 0.0001 m, $d_0$ = 0.0000503 m | $\varepsilon_r$ = 3.2, $d$ = 0.0001 m, $d_0$ = 0.00003125 m |
| area size of dielectrics $S$ | 0.005 $m^2$ | 0.005 $m^2$ |
| maximum separation distance, $x_{max}$ | 0.004 m | 0.004 m |
| tribo surface charge density, $\sigma$[68,69] | 10 $\mu$C $m^{-2}$ | 0.85 mC $m^{-2}$ |
| velocity $v$ | 0.1 $ms^{-1}$ | 0.1 1 $ms^{-1}$ |
| $V_{TENG}$ | $1.1294 \times 10^6 x(t)$ V | $0.0960 \times 10^9 x(t)$ V |
| $V_{OCMAX}$ | 2.2 kV | 192 kV |
| $C_{TENG}$ | $\frac{4.427 \times 10^{-14}}{5.03 \times 10^{-5} + x(t)}$ | $\frac{4.427 \times 10^{-14}}{3.13 \times 10^{-5} + x(t)}$ |
| $C_{TENG,MAX}$ | $89 \times 10^{-10}$ F | $142 \times 10^{-9}$ F |
| $C_{TENG,MIN}$ | $2 \times 10^{-11}$ F | $2 \times 10^{-11}$ F |

In reference to the equivalent circuit of TENG (Figure 6d), the equivalent voltage source is a function of conductivity, dielectric constant, and the separation distance $x$. So we could simulate the voltage profile for both PVA and PAN nanofiber membranes as dielectric layers by fixing the maximum distance between the electrodes as 4 mm. The other parameters used to simulate is given in Table 1. The simulated circuit is referenced in Figure 7a.

$V_{TENG}$ of the dielectric layer in the system can be obtained using the equation, $V_{TENG} = \frac{\sigma}{\varepsilon_0} x(t)$ and their parameter values from Table 1.

The equivalent voltage is as follows:

for the PVA dielectric layer, $V_{TENG} = 1.1294 \times 10^6\ x(t)$

for the PAN dielectric layer, $V_{TENG} = 0.0960 \times 10^9\ x(t)$

Since we consider a periodic load with a maximum velocity of 0.1 $ms^{-1}$, we could get a maximum output, i.e., $V_{OCMax}$ as 2.2 kV and 192 kV for PVA and PAN dielectric layers, respectively. 0.1 $ms^{-1}$ is the typical wind speed that can be exerted by a normal human being during the breathing process. The profile of the graph is shown in Figure 7b,c. We consider a sinusoidal oscillation of the TENG at a frequency of 25 Hz. The voltage generated becomes dependent on the periodic oscillation of the dielectric layer.

Based on the assumption that the vibration is periodic in nature, we simulated the TENG structure by subjecting it to the same. The period of vibration was taken as 25 Hz which is a similar range to a human heartbeat.

The TENG with a periodic input can be modeled as a voltage dependent voltage source as shown in Figure 8a. This will make $V_{TENG}$ and $C_{TENG}$ parameters dependent on the periodic movement.

Based on the eqs 8 and 9, $C_{TENG}$ and $V_{TENG}$ of the capacitor voltage ($V_c$) of the TENG system is independent of the charge density of the dielectric layer. $V_c$ of the system with PVA and PAN dielectric layer for different charge densities has been simulated.

The variable capacitance $C_{TENG}$ is a function of the surface area (actual) and the relative distance between the electrodes and the dielectric layer.

We calculated the same values for the frequency and contact area of 5 $mm^2$. The initial capacitance is found to be $89 \times 10^{-10}$ and $2 \times 10^{-11}$ F for PVA and PAN respectively. The corresponding maximum voltages of the capacitor ($V_c$) are 2.2 kV and 192 kV for PVA and PAN respectively as shown in Figure 8(i)-b,c. and are equal to their $V_{OCMAX}$ values. We assume that the entire surface is in contact with the electrode, as shown in Figure 7a. By utilizing the parameter values in Table 1 with the equation $C_{TENG} = \frac{\varepsilon_0 S}{d_0 + x(t)}$, the $C_{TENG}$ of the system of both PVA and PAN dielectric layers can be calculated as follows:

for the PVA dielectric layer, $C_{TENG} = \frac{4.427 \times 10^{-14}}{5.03 \times 10^{-5} + x(t)}$

for the PAN dielectric layer, $C_{TENG} = \frac{4.427 \times 10^{-14}}{3.13 \times 10^{-5} + x(t)}$

By applying the $x(t)$ value from zero to maximum, it is observed that when the $x(t)$ is 0, the triboelectric capacitance reaches a maximum value, and when the $x(t)$ is maximum, the capacitance value will be minimum.

Figure 8(ii) shows the voltage across the resistor ($V_r$) for resistance of 1 and 10 GΩ, that drops to the minimum value (zero) after the transients. The steady state was attained much earlier with a load of 1 GΩ for both membranes. This is due to the time constant (RC) of the circuit, whereas it takes 1 s to reach the steady state for a load resistance of 10 GΩ. Figure 8(ii)d,e shows the $V_r$ peak for $R$ = 1 GΩ for PVA and PAN dielectric layers, and Figure 8(ii)f,g shows the peak for $R$ = 10 GΩ for PVA and PAN. It is observed that the $V_r$ decreases when $R$ increases; it represents the increase in charging time.

To know the effect of variation in the load and the power transferred to the load. We varied the load from 100 kΩ to 100 MΩ. Figure 9a,b. shows that upon increasing the resistance, the voltage values will be increased as 680 V for PVA and 57 kV for the PAN dielectric layer, respectively. Figure 9c,d shows that the current decreases as the resistance increases . The



https://doi.org/10.1021/acsomega.4c03625
ACS Omega 2024, 9, 37802−37813

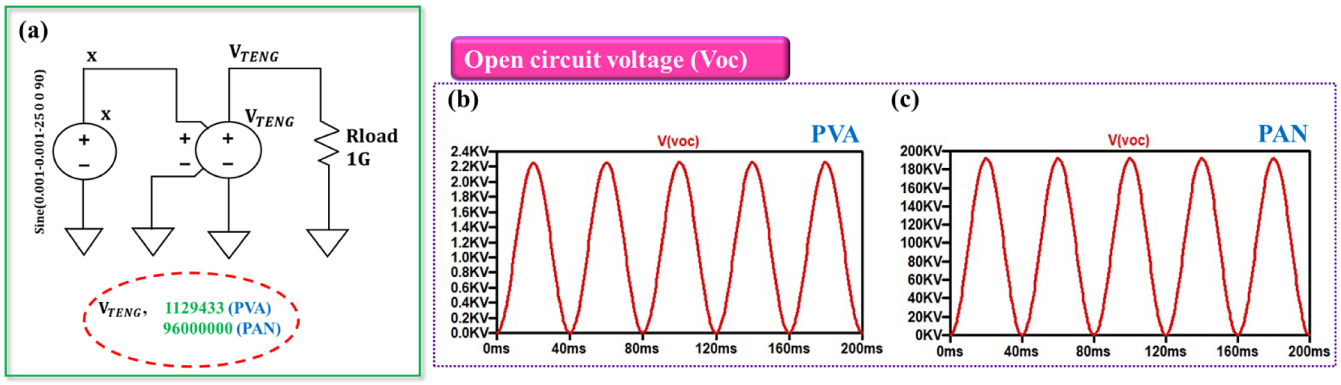


**Figure 7.** (a) LTspice circuit of voltage−controlled voltage source. (b,c) Simulation of open circuit voltage of PVA and PAN dielectric layers.

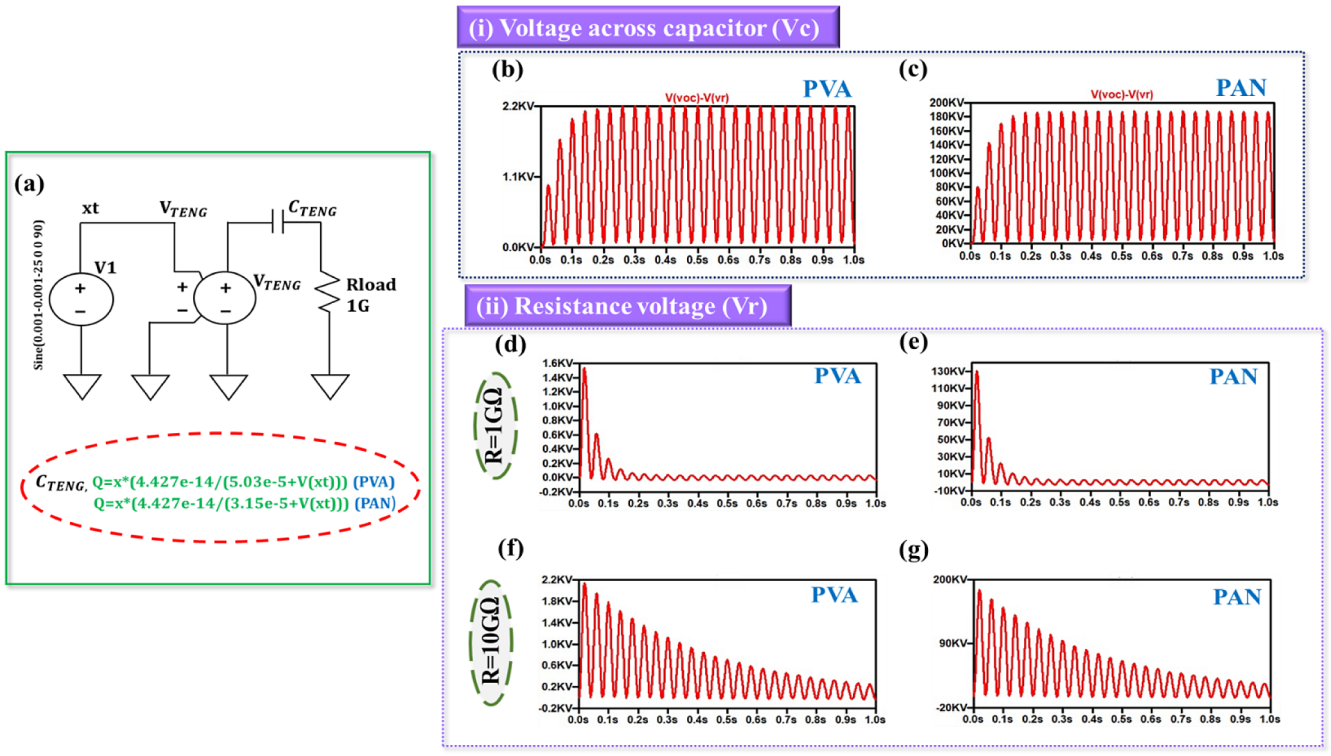


**Figure 8.** (a) Schematic of TENG system. (i) Simulation of voltage across capacitor for (b) PVA and (c) PAN dielectric layers. (ii) The voltage across the load resistance for PVA and PAN dielectric layers with *R* of (d,e) 1 GΩ and (f,g) 10 GΩ.

maximum current of TENG is achieved at the lowest resistance of 100 kΩ as 16.5 μA and 1.8 mA for PVA and PAN respectively. The maximum power transfer happened at 100 MΩ for both membranes.

The calculated power generation of these membranes reaches 0.004624 W (PVA) and 32.49 W (PAN).

*3.2.3. Energy Harvesting from Other Sources.* Similarly, we have analyzed a wide range of wasted mechanical energy sources and their corresponding energy produced. Table 2 reveals the obtained results under different ranges of frequencies. It starts from a minimum frequency of 0.16 Hz (human breath) to a maximum frequency of 50 Hz (engine idling). With a suitable load, the minimum output power of PVA and PAN is calculated as 0.000121 and 0.0121 W respectively at 0.16 Hz, and the maximum output power as 0.6561 W (PVA) and 39.69 W (PAN) at 50 Hz. The minimum power generation of both membranes can be used for powering portable electronic gadgets.

## 4. DISCUSSION

Since we assumed a free-standing membrane as a dielectric layer which oscillates between two metal electrodes, the output is also alternative in nature. The membrane's mechanical behaviors such as Young's modulus and spring constant decide the nature of the oscillations produced due to certain loads acting on the TENG. The membrane can be modeled as a second order system, and it can be tuned properly to give a vibration-free oscillation. This vibration-free oscillation results in a ripple free voltage that can enhance the quality of the voltage generated. This is possible by keeping the damping factor close to one. In terms of electrical characteristics, the charge density plays a major role in the conversion process. Since we used bare PVA and PAN solutions, there is a possibility of improving the electrical output by making composites with metal nanoparticles.



https://doi.org/10.1021/acsomega.4c03625
ACS Omega 2024, 9, 37802−37813

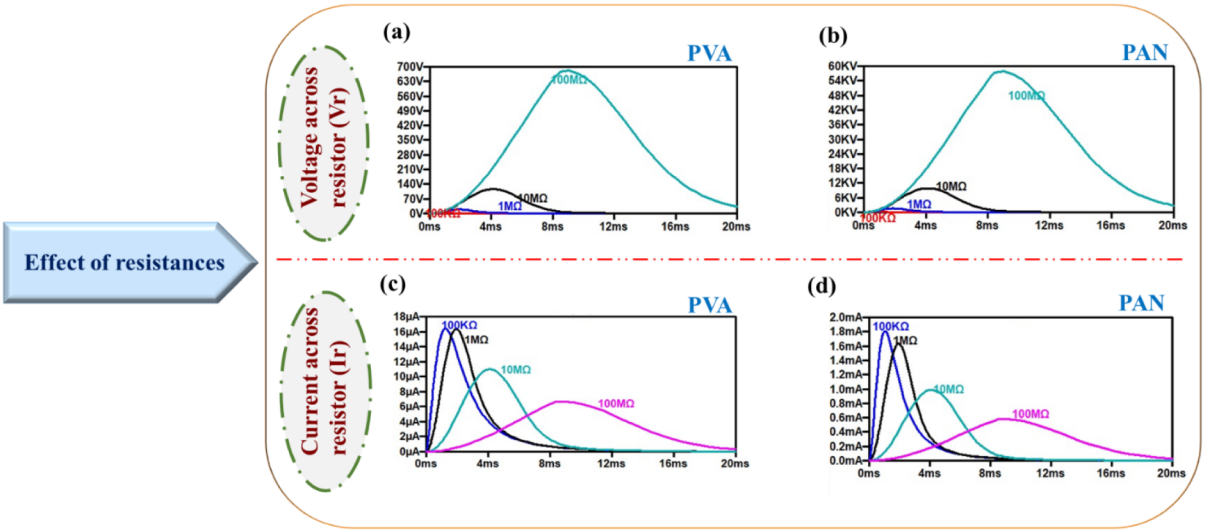


**Figure 9.** Effect of load resistances. (a,b) Voltage across the load resistor. (c,d) Current through the load resistor.

**Table 2. Simulated Results of Power Harvested from Other Sources of Vibration**

| | | Power generated (W) | |
|---|---|---|---|
| vibration sources | frequency (Hz) | PVA nanofiber membrane | PAN nanofiber membrane |
| normal respiration rate of human (10–20 breaths/min) | 0.16–0.33 | 0.000121–0.000441 | 0.0121–0.0441 |
| human motion[70] | 1–3 | 0.003025–0.014641 | 0.3025–1.2769 |
| walking (60 steps/min) | 1 | 0.003025 | 0.3025 |
| jogging (90 steps/min) | 1.5 | 0.005476 | 0.5041 |
| running slowly (120 steps/min) | 2 | 0.008281 | 0.7396 |
| running quickly (180 steps/min) | 3 | 0.014641 | 1.2769 |
| hand tapping | 4–5 | 0.0256–0.038025 | 1.8225–2.56 |
| water waves of low frequency | 1–2 | 0.003025–0.008281 | 0.3025–0.7396 |
| engine shake (Idling vibration) | 20–50 | 0.2025–0.6561 | 14.44–39.69 |

The TENG should be in a position to be an independent power source. So we extended our study by connecting various loads. As a basic law, the source resistance should be equal to the load resistance to deliver the maximum power. We tried to extend the study further by correlating various sources of vibration and their corresponding power generation capacities. Our analysis shows that the spun PVA membrane has random nanofiber orientation, whereas the PAN membrane has aligned nanofibers. Due to their orientation, the mechanical properties of the PAN membrane are higher than those of the PVA membrane. In the theoretical results of CFTENG, the output voltage of the PAN membrane was achieved as 192 kV due to its charge density (0.85 mC $m^{-2}$), whereas the PVA membrane has 2.2 kV. Hence, the spun dielectric layer of PAN nanofiber membrane offers a good approach in energy harvesting technologies. All the above-mentioned analyses can be realized with suitable hardware.

## 5. CONCLUSION

Energy harvesting from ambient vibrational sources can be carried out by using triboelectric materials. We report an experiment based on PVA and PAN nanofiber membranes that are used as a dielectric layer in TENGs. We carried out the mechanical analysis of PVA and PAN nanofiber membranes spun by the electrospinning method based on the representative volume element (RVE) method. The fibers in the membrane are uniform in size, and the orientation of the fibers is narrow for the PAN nanofiber membrane. PVA membrane has the random nanofiber orientation, whereas PAN membrane has aligned nanofibers. Due to their orientation, the mechanical properties of the PAN membrane are higher than those of the PVA membrane. The mechanical analysis showed a good response for certain loads and damping. In the comparison to the maximum open-circuit voltage, the PAN membrane generated 192 kV because of a higher charge density (0.85 mC $m^{-2}$), whereas the PVA membrane could generate 2.2 kV. So, the spun dielectric layer of PAN nanofiber membrane offers a good approach in energy harvesting technologies. The modeling is extended to other sources of vibrations, and the energy supplied is also estimated.

## AUTHOR INFORMATION


### Corresponding Author

**Velmurugan Venugopal** − *Department of Micro and Nanoelectronics, School of Electronics Engineering, Vellore Institute of Technology, Vellore, Tamil Nadu 632014, India;* orcid.org/0000-0001-7893-4514; Email: vvelmurugan@vit.ac.in

### Author

**Subalakshmi Pragalathan** − *Department of Chemistry, School of Advanced Sciences, Vellore Institute of Technology, Vellore, Tamil Nadu 632014, India*

Complete contact information is available at: https://pubs.acs.org/10.1021/acsomega.4c03625


### Notes

The authors declare no competing financial interest.



https://doi.org/10.1021/acsomega.4c03625
*ACS Omega* 2024, 9, 37802−37813

## ■ ACKNOWLEDGMENTS

The authors would like to acknowledge Vellore Institute of Technology (VIT), Vellore for providing us the support in publishing this paper, Centre for Nanotechnology Research, VIT, Vellore for providing lab facilities to carry out the experimental work. Further, the authors wish to thank CeNSE, Indian Institute of Science, Bengaluru, funded by the Ministry of Human Resource Development (MHRD), Ministry of Electronics and Information Technology (MeitY), and Nano-mission, Department of Science and Technology (DST), Govt. of India for SEM characterization.

## ■ REFERENCES

(1) Liu, G.; Yu, Y.; Hou, J.; Xue, W.; Liu, X.; Liu, Y.; Wang, W.; Alsaedi, A.; Hayat, T.; Liu, Z. An Ecological Risk Assessment of Heavy Metal Pollution of the Agricultural Ecosystem near a Lead-Acid Battery Factory. *Ecol. Indic.* **2014**, *47*, 210−218.

(2) Melchor-Martínez, E. M.; Macias-Garbett, R.; Malacara-Becerra, A.; Iqbal, H. M. N.; Sosa-Hernández, J. E.; Parra-Saldívar, R. Environmental Impact of Emerging Contaminants from Battery Waste: A Mini Review. *Case Stud. Chem. Environ. Eng.* **2021**, *3*, 100104.

(3) Liu, H.; Fu, H.; Sun, L.; Lee, C.; Yeatman, E. M. Hybrid Energy Harvesting Technology: From Materials, Structural Design, System Integration to Applications. *Renewable Sustainable Energy Rev.* **2021**, *137*, 110473.

(4) Cheng, T.; Shao, J.; Wang, Z. L. Triboelectric Nanogenerators. *Nat. Rev. Methods Primers* **2023**, *3* (1), 39.

(5) Panda, S.; Hajra, S.; Song, H.; Jo, J.; Kim, N.; Hwang, S.; Choi, Y.; Kim, H. G.; Kim, H. J.; Mishra, Y. K. Pyroelectric Based Energy Harvesting Devices: Hybrid Structures and Applications. *Sustain. Energy Fuels* **2023**, *7* (22), 5319−5335.

(6) Qu, Z.; Wang, X.; Huang, M.; Chen, C.; An, Y.; Yin, W.; Li, X. An Eccentric-Structured Hybrid Triboelectric-Electromagnetic Nanogenerator for Low-Frequency Mechanical Energy Harvesting. *Nano Energy* **2023**, *107*, 108094.

(7) Bairagi, S.; Shahadat, M.; Mulvihill, D.M.; Ali, W. Mechanical Energy Harvesting and Self-Powered Electronic Applications of Textile-Based Piezoelectric Nanogenerators: A Systematic Review. *Nano Energy* **2023**, *111*, 108414.

(8) Fan, F. R.; Tian, Z. Q.; Lin Wang, Z. Flexible Triboelectric Generator. *Nano Energy* **2012**, *1* (2), 328−334.

(9) Zhu, G.; Chen, J.; Zhang, T.; Jing, Q.; Wang, Z. L. Radial-Arrayed Rotary Electrification for High Performance Triboelectric Generator. *Nat. Commun.* **2014**, *5*, 5.

(10) Wu, C.; Wang, A. C.; Ding, W.; Guo, H.; Wang, Z. L.Triboelectric Nanogenerator: A Foundation of the Energy for the New Era*Advanced Energy Materials*; Wiley-VCH Verlag, 2019, Vol. 3. .

(11) He, X.; Zi, Y.; Yu, H.; Zhang, S. L.; Wang, J.; Ding, W.; Zou, H.; Zhang, W.; Lu, C.; Wang, Z. L. An Ultrathin Paper-Based Self-Powered System for Portable Electronics and Wireless Human-Machine Interaction. *Nano Energy* **2017**, *39*, 328−336.

(12) Xu, G.; Li, C.; Chen, C.; Fu, J.; Hou, T.; Zi, Y. Dynamics of Triboelectric Nanogenerators: A Review. In *International Journal of Mechanical System Dynamics*; John Wiley and Sons Inc, 2022; pp. 311324. .

(13) Karan, S. K.; Maiti, S.; Lee, J. H.; Mishra, Y. K.; Khatua, B. B.; Kim, J. K. Recent Advances in Self-Powered Tribo-/Piezoelectric Energy Harvesters: All-In-One Package for Future Smart Technologies. In *Advanced Functional Materials*; Wiley-VCH Verlag, 2020..

(14) Duan, Q.; Peng, W.; He, J.; Zhang, Z.; Wu, Z.; Zhang, Y.; Wang, S.; Nie, S. Rational Design of Advanced Triboelectric Materials for Energy Harvesting and Emerging Applications. *Small Methods* **2023**, *7* (2), 2201251.

(15) Wang, S.; Lin, Z.-H.; Niu, S.; Lin, L.; Xie, Y.; Pradel, K. C.; Wang, Z. L. Motion Charged Battery as Sustainable Flexible-Power-Unit. *ACS Nano* **2013**, *7* (12), 11263−11271.

(16) Wang, Y.; Yang, Y.; Wang, Z. L. Triboelectric Nanogenerators as Flexible Power Sources. *Npj Flex. Electron.* **2017**, *1* (1), 10.

(17) Pu, X.; Zhang, C.; Wang, Z. L. Triboelectric Nanogenerators as Wearable Power Sources and Self-Powered Sensors. *Natl. Sci. Rev.* **2023**, *10* (1), nwac170.

(18) Niu, S.; Liu, Y.; Chen, X.; Wang, S.; Zhou, Y. S.; Lin, L.; Xie, Y.; Wang, Z. L. Theory of Freestanding Triboelectric-Layer-Based Nanogenerators. *Nano Energy* **2015**, *12*, 760−774.

(19) Chen, B.; Yang, Y.; Wang, Z. L. Scavenging Wind Energy by Triboelectric Nanogenerators. In *Advanced Energy Materials*; Wiley-VCH Verlag, 2018..

(20) Ren, Z.; Wu, L.; Pang, Y.; Zhang, W.; Yang, R. Strategies for Effectively Harvesting Wind Energy Based on Triboelectric Nanogenerators. In *Nano Energy*; Elsevier Ltd, 2022..

(21) Chen, A.; Zhang, C.; Zhu, G.; Wang, Z. L. Polymer Materials for High-Performance Triboelectric Nanogenerators. In *Advanced Science*; John Wiley and Sons Inc, 2020..

(22) Dong, K.; Peng, X.; Cheng, R.; Wang, Z. L. Smart Textile Triboelectric Nanogenerators: Prospective Strategies for Improving Electricity Output Performance. *Nanoenergy Adv.* **2022**, *2* (1), 133−164.

(23) Seol, M.-L.; Lee, S.-H.; Han, J.-W.; Kim, D.; Cho, G.-H.; Choi, Y.-K. Impact of Contact Pressure on Output Voltage of Triboelectric Nanogenerator Based on Deformation of Interfacial Structures. *Nano Energy* **2015**, *17*, 63−71.

(24) Jin, C.; Kia, D. S.; Jones, M.; Towfighian, S. On the Contact Behavior of Micro-/Nano-Structured Interface Used in Vertical-Contact-Mode Triboelectric Nanogenerators. *Nano Energy* **2016**, *27*, 68−77.

(25) Babu, A.; Aazem, I.; Walden, R.; Bairagi, S.; Mulvihill, D. M.; Pillai, S. C. Electrospun Nanofiber Based TENGs for Wearable Electronics and Self-Powered Sensing. *Chem. Eng. J.* **2023**, *452*, 139060.

(26) Ge, X.; Hu, N.; Yan, F.; Wang, Y. Development and Applications of Electrospun Nanofiber-Based Triboelectric Nanogenerators. In *Nano Energy*; Elsevier Ltd, 2023..

(27) Wang, Q.; Ma, J.; Chen, S.; Wu, S. Designing an Innovative Electrospinning Strategy to Generate PHBV Nanofiber Scaffolds with a Radially Oriented Fibrous Pattern. *Nanomaterials* **2023**, *13* (7), 1150.

(28) Khan, Y.; Garg, M.; Gui, Q.; Schadt, M.; Gaikwad, A.; Han, D.; Yamamoto, N. A.; Hart, P.; Welte, R.; Wilson, W.; Czarnecki, S. Flexible Hybrid Electronics: Direct Interfacing of Soft and Hard Electronics for Wearable Health Monitoring. *Adv. Funct. Mater.* **2016**, *26* (47), 8764−8775.

(29) Diaz, A. F.; Felix-Navarro, R. M. A Semi-Quantitative Tribo-Electric Series for Polymeric Materials: The Influence of Chemical Structure and Properties. *J. Electrostat.* **2004**, *62* (4), 277−290.

(30) Mohsen, M.; Abdel Gaber, S. A.; Shoueir, K. R.; El-Kemary, M.; Abo El-Yazeed, W. S. Synthesis of Cross-Linked and Sterilized Water-Soluble Electrospun Nanofiber Biomatrix of Streptomycin-Imbedded PVA/CHN/$\beta$-CD for Wound Healing. *ACS Omega* **2024**, *9* (9), 10058−10068.

(31) Taborda, M. I.; Catalan, K. N.; Orellana, N.; Bezjak, D.; Enrione, J.; Acevedo, C. A.; Corrales, T. P. Micropatterned Nanofiber Scaffolds of Salmon Gelatin, Chitosan, and Poly(Vinyl Alcohol) for Muscle Tissue Engineering. *ACS Omega* **2023**, *8* (50), 47883−47896.

(32) Zhai, Z.; Wang, X.; Huang, Y.; Zhao, Y. Fabrication of Phenolic Resin Membrane with Polyvinyl Alcohol Fiber Skeleton by Electrospinning for Organic Solvent Nanofiltration. *Sep. Purif. Technol.* **2024**, *332*, 125852.

(33) Yue, W.; Ren, L.; Dong, Y.; Dan, Y.; Cao, Y.; Liang, H.; Zhu, S.; Zhu, L.; Liu, F.; He, J.; Shao, W. Green Continuous Electrospinning to Fabricate Multiscale Chitosan Nanofibers by Regulating of Polyvinyl Alcohol for Mask Filter Applications. *ACS Appl. Polym. Mater.* **2024**, *6* (5), 2954−2963.

(34) Bai, X.; Luan, J.; Song, T.; Sun, H.; Yan, B.; Dai, Y.; Yu, J. Polyvinyl Alcohol/Polyethyleneimine Grafted Carbon Oxynitride Composite Nanofiber Membranes with the Synergistical Enhanced



https://doi.org/10.1021/acsomega.4c03625
*ACS Omega* 2024, 9, 37802−37813

Photocatalytic Degradation and Bactericidal Performance. *J. Appl. Polym. Sci.* **2024**, *141*, No. e55699.
(35) Kang, L.; Ma, C.; Wang, J.; Gao, X.; An, G. PTFE/PVA-PVDF Conjugated Electrospun Nanofiber Membrane with Triboelectric Effect Used in Face Mask. *Fibers Polym.* **2023**, *24* (6), 1975−1982.
(36) Peng, X.; Dong, K.; Ye, C.; Jiang, Y.; Zhai, S.; Cheng, R.; Liu, D.; Gao, X.; Wang, J.; Lin Wang, Z. *A Breathable, Biodegradable, Antibacterial, and Self-Powered Electronic Skin Based on All-Nanofiber Triboelectric Nanogenerators*; 2020. https://www.science.org.
(37) Sun, W.; Ji, G.; Chen, J.; Sui, D.; Zhou, J.; Huber, J. Enhancing the Acoustic-to-Electrical Conversion Efficiency of Nanofibrous Membrane-Based Triboelectric Nanogenerators by Nanocomposite Composition. *Nano Energy* **2023**, *108*, 108248.
(38) Yang, Y.; Yang, Y.; Huang, J.; Li, S.; Meng, Z.; Cai, W.; Lai, Y. Electrospun Nanocomposite Fibrous Membranes for Sustainable Face Mask Based on Triboelectric Nanogenerator with High Air Filtration Efficiency. *Adv. Fiber Mater.* **2023**, *5* (4), 1505−1518.
(39) Arica, T. A.; Isık, T.; Guner, T.; Horzum, N.; Demir, M. M. Advances in Electrospun Fiber-Based Flexible Nanogenerators for Wearable Applications. In *Macromolecular Materials and Engineering*; John Wiley and Sons Inc, 2021..
(40) Zhao, S.; Wang, J.; Du, X.; Wang, J.; Cao, R.; Yin, Y.; Zhang, X.; Yuan, Z.; Xing, Y.; Pui, D. Y. H.; et al. All-Nanofiber-Based Ultralight Stretchable Triboelectric Nanogenerator for Self-Powered Wearable Electronics. *ACS Appl. Energy Mater.* **2018**, *1* (5), 2326−2332.
(41) Venkatesan, H. M.; Arun, A. P. Nickel-Oxide-Doped Polyvinylidene Fluoride Nanofiber-Based Flexible Triboelectric Nanogenerator for Energy Harvesting and Healthcare Monitoring Applications. *ACS Appl. Electron. Mater.* **2024**, *6* (2), 1161−1173.
(42) Shi, B.; Wang, Q.; Su, H.; Li, J.; Xie, B.; Wang, P.; Qiu, J.; Wu, C.; Zhang, Y.; Zhou, X.; et al. Progress in Recent Research on the Design and Use of Triboelectric Nanogenerators for Harvesting Wind Energy. *Nano Energy* **2023**, *116*, 108789.
(43) Tan, E. P. S.; Ng, S. Y.; Lim, C. T. Tensile Testing of a Single Ultrafine Polymeric Fiber. *Biomaterials* **2005**, *26* (13), 1453−1456.
(44) Maruccio, C.; De Lorenzis, L.; Persano, L.; Pisignano, D. Computational Homogenization of Fibrous Piezoelectric Materials. *Comput. Nanomech.* **2015**, *55* (5), 983−998.
(45) Chanda, A.; Sinha, S. K.; Datla, N. V. The Influence of Fiber Alignment, Structure and Concentration on Mechanical Behavior of Carbon Nanofiber/Epoxy Composites: Experimental and Numerical Study. *Polym. Compos.* **2021**, *42* (3), 1155−1173.
(46) Jia, C.; Zhang, T.; Zhao, H. A Computational Micromechanics Model to Predict Mechanical Properties of Porous Silica Aerogels. *J. Appl. Phys.* **2022**, *132*, 15, DOI:.
(47) Yu, N.; Ma, H.; Wu, C.; Yu, G.; Yan, B. Modeling and Experimental Investigation of a Novel Bistable Two-Degree-of-Freedom Electromagnetic Energy Harvester. *Mech Syst. Signal Process* **2021**, *156*, 107608.
(48) Fu, Y.; Ouyang, H.; Davis, R. B. Triboelectric Energy Harvesting from the Vibro-Impact of Three Cantilevered Beams. *Mech. Syst. Signal Process* **2019**, *121*, 509−531.
(49) Li, L.; Hsieh, Y.-L. Ultra-Fine Polyelectrolyte Hydrogel Fibres from Poly (Acrylic Acid)/Poly (Vinyl Alcohol). *Nanotechnology* **2005**, *16* (12), 2852.
(50) Phachamud, T.; Phiriyawirut, M. Physical Properties of Polyvinyl Alcohol Electrospun Fiber Mat. *Res. J. Pharm. Biol. Chem. Sci.* **2011**, *2*, 675−684.
(51) Bakar, S. S. S.; Foong, K. M.; Halif, N. A.; Yahud, S. Effect of Solution Concentration and Applied Voltage on Electrospun Polyacrylonitrile Fibers. In *IOP Conference Series: materials Science and Engineering*; IOP Publishing; 2019, Vol. *701*, pp: 012018.
(52) Maciel, M. M.; Ribeiro, S.; Ribeiro, C.; Francesko, A.; Maceiras, A.; Vilas, J. L.; Lanceros-Méndez, S. Relation between Fiber Orientation and Mechanical Properties of Nano-Engineered Poly-(Vinylidene Fluoride) Electrospun Composite Fiber Mats. *Compos. B Eng.* **2018**, *139*, 146−154.
(53) Nitti, P.; Gallo, N.; Natta, L.; Scalera, F.; Palazzo, B.; Sannino, A.; Gervaso, F. Influence of Nanofiber Orientation on Morphological and Mechanical Properties of Electrospun Chitosan Mats. *J. Healthc. Eng.* **2018**, *2018*, 3651480.
(54) Rudra, S.; Janani, K.; Thamizharasan, G.; Pradhan, M.; Rani, B.; Sahu, N.K.; Nayak, A.K. Fabrication of Mn3O4-WO3 Nanoparticles Based Nanocomposites Symmetric Supercapacitor Device for Enhanced Energy Storage Performance under Neutral Electrolyte. *Electrochim. Acta* **2022**, *406*, 139870.
(55) Jin, H.; Sun, G.; Zhang, B.; Luo, N.; Li, Y.; Lin, L.; Bala, H.; Cao, J.; Zhang, Z.; Wang, Y. Facile Synthesis of Co3O4 Nanochains and Their Improved TEA Sensing Performance by Decorating with Au Nanoparticles. *J. Alloys Compd.* **2019**, *776*, 782−790.
(56) Rani, B.; Nayak, A. K.; Sahu, N. K. Electrochemical Supercapacitor Application of CoFe2O4 Nanoparticles Decorated over Graphitic Carbon Nitride. *Diam. Relat. Mater.* **2021**, *120*, 108671.
(57) El Moumen, A.; Kanit, T.; Imad, A. Numerical Evaluation of the Representative Volume Element for Random Composites. *Eur. J. Mech.-A/solids* **2021**, *86*, 104181.
(58) Pike, M. G.; Oskay, C. Modeling Random Short Nanofiber-and Microfiber-Reinforced Composites Using the Extended Finite-Element Method. *J. Nanomech. Micromech.* **2015**, *5* (1), A4014005.
(59) Yin, Y.; Pu, D.; Xiong, J. Analysis of the Comprehensive Tensile Relationship in Electrospun Silk Fibroin/Polycaprolactone Nanofiber Membranes. *Membranes* **2017**, *7* (4), 67.
(60) Xiao, X.; Long, A.; Lin, H.; Zeng, X. Large Deformation Modelling of Tight Woven Fabric under High Air Pressure. *J. Eng. Fiber. Fabr.* **2015**, *10* (3), 155892501501000107.
(61) Xiao, X.; Long, A.; Zeng, X. Through-Thickness Permeability Modelling of Woven Fabric under out-of-Plane Deformation. *J. Mater. Sci.* **2014**, *49* (21), 7563−7574.
(62) Ibrahim, A.; Ramini, A.; Towfighian, S. Modeling an Impact Vibration Harvester with Triboelectric Transduction. In *Proceedings Of The ASME Design Engineering Technical Conference*, ASME, 2017.
(63) Ibrahim, A.; Ramini, A.; Towfighian, S. Experimental and Theoretical Investigation of an Impact Vibration Harvester with Triboelectric Transduction. *J. Sound Vib.* **2018**, *416*, 111−124.
(64) Cao, X.; Chen, W.; Zhao, P.; Yang, Y.; Yu, D.-G. Electrospun Porous Nanofibers: Pore− Forming Mechanisms and Applications for Photocatalytic Degradation of Organic Pollutants in Wastewater. *Polymers* **2022**, *14* (19), 3990.
(65) AmorosoJothi, S.; JothiPandiarajan, J.; PandiarajanLakshmipriya, V.; Lakshmipriya Prithivikumaran, N.; Prithivikumaran Natarajan, B.; NatarajanJeyakumaran, N. Determination of optical, elastic, and acoustical properties of porous silicon as a function of anodization current density. *Spec. Top. Rev. Porous Media* **2014**, *5* (1), 53−62.
(66) Niu, S.; Zhou, Y. S.; Wang, S.; Liu, Y.; Lin, L.; Bando, Y.; Wang, Z. L. Simulation Method for Optimizing the Performance of an Integrated Triboelectric Nanogenerator Energy Harvesting System. *Nano Energy* **2014**, *8*, 150−156.
(67) Niu, S.; Liu, Y.; Wang, S.; Lin, L.; Zhou, Y. S.; Hu, Y.; Wang, Z. L. Theory of Sliding-Mode Triboelectric Nanogenerators. *Adv. Mater.* **2013**, *25* (43), 6184−6193.
(68) Liu, D.; Liu, J.; Yang, M.; Cui, N.; Wang, H.; Gu, L.; Wang, L.; Qin, Y. Performance Enhanced Triboelectric Nanogenerator by Taking Advantage of Water in Humid Environments. *Nano Energy* **2021**, *88*, 106303.
(69) Wang, J.; Wu, H.; Fu, S.; Li, G.; Shan, C.; He, W.; Hu, C. Enhancement of Output Charge Density of TENG in High Humidity by Water Molecules Induced Self-Polarization Effect on Dielectric Polymers. *Nano Energy* **2022**, *104*, 107916.
(70) Tan, Y.; Zhang, Y.; Ren, L. Energy Harvesting from an Artificial Bone. *IEEE Access* **2019**, *7*, 120065−120075.


https://doi.org/10.1021/acsomega.4c03625
*ACS Omega* 2024, 9, 37802−37813